Lithuanian Journal of Physics
Vol. **65**, No. 4, pp. 194–202 (2025)
ISSN 1648-8504 eISSN 2424-3647
DOI: https://doi.org/10.3952/physics.2025.65.4.2

CLASSIFICATION OF CONCEALED OBJECTS USING TERAHERTZ IMAGING AND ARTIFICIAL NEURAL NETWORKS

U. Šilingaitė and I. Grigelionis

Center for Physical Sciences and Technology, Saulėtekio 3, 10257 Vilnius, Lithuania
Email: ugne.silingaite@ftmc.lt

Received 29 November 2025; accepted 3 December 2025

Imaging in the terahertz frequency band is applied in a number of fields, such as security, medical or quality control. However, a low resolution or distortions of the images hinder the identification or recognition of the objects. To cope with the processing of visual information, artificial neural networks are broadly employed. In this work, the monochromatic radiation of 253 GHz was used to collect the image set of the investigated objects either in the air or covered with a packing material. Such a set was later used to train convolutional and generative adversarial neural networks poised for three tasks: (i) the classification of objects; (ii) the enhancement of image resolution; (iii) the identification of cover material. The obtained results demonstrated that the packaging materials were identified with an accuracy of 83.33%, while the investigated objects were classified with an accuracy of 89.42%. The PSNR metric of images with improved resolution reached up to 22.44 dB. The optical properties such as refractive indices and absorption coefficients of the packaging materials were also defined using terahertz time-domain spectroscopy, and it was found that the accuracy of object and material classification in general does not depend on the physical properties and type of a package.

Keywords: terahertz imaging, neural networks, image processing

1. Introduction

One of the most prominent applications of terahertz (THz) waves (electromagnetic range from 100 GHz to 10 THz) was found to be THz imaging of various materials and objects [1, 2]. Since THz radiation penetrates dielectric materials [3–5], it can be employed for non-invasive packaging inspection while searching for concealed objects [6, 7]. Moreover, organic materials have their spectral footprints in the THz range, therefore such radiation can be used in the identification of drugs and plastic explosives [8, 9], gas sensing [10] or cancer diagnostics [11]. The wavelength of the THz waves typically used for imaging is in the order of millimetres or sub-millimetres. Therefore, the spatial resolution of the image is limited, leading to limitations in detectable object size and edge sharpness. What is more, if the object is concealed by some sort of packaging material, then the absorption/reflection of THz waves by the material lowers the signal-to-noise ratio and thus the contrast of the image significantly deteriorates. In the simplest THz imaging approach – a direct THz imaging, an object is placed in the focus of the THz beam coming from the source, and the signal is registered in transmission and/or reflection geometries. In this case, to ensure image quality, it is crucial that the investigated object stays in the focus plane all the time. Moreover, low-frequency commercial THz sources are more compact, user-friendly, and have higher optical output power, but suffer from limited spatial resolution in imaging applications. As an example, field-effect transistor-based sources can operate at 253 GHz at room temperature, and still be relatively compact [12]. On the other hand, if, for example, the edges of the objects need to be emboldened, dark-field imaging might be a solution [13]; however, the additional complexity of filter selection and positioning arises, and the problem of correct sample placement persists.

Artificial neural networks (ANN) allow for extended capabilities in image processing. Starting from the original idea of employing the perceptron algorithm [14] and adding the contemporary calculation resources, the applications of artificial neural networks (ANNs) are expanding rapidly, offering a plethora of new tools and applications.

ANNs are successfully applied in computer vision, mostly on visible light images, where a fast processing of large amounts of data is required. For such tasks, convolutional neural networks [15] are often used. In THz imaging, ANNs are used for automatic edge and feature detection [16], which, however, represents only a small fraction of processing tasks that can be performed. It is worth noting that attempts have been made to use neural networks to increase the resolution of terahertz images [17, 18]. Most efforts of THz image processing with ANNs are constrained to imaging of uncovered objects, thus employing the well-established ANN models to the image processing of concealed objects makes it an attractive subject of study.

In this work, different models of artificial neural networks are employed for the tasks of object classification, spatial image resolution improvement, and package material recognition from a set of monochromatic THz images obtained at 253 GHz frequency. The set of 276 raw THz images was collected, which was later augmented by digitally applying such transformations as mirror reflection and rotations. Also, a part of those images was of objects covered with various packaging materials. Terahertz time-domain spectroscopy was also used to determine the optical properties of those materials at 253 GHz. The precision as high as 89.42 and 83.33% for object and shielding material classification, respectively, were reached. Also, the peak signal-to-noise ratio (PSNR) values of the images with increased spatial resolution reached 22.44 dB. The obtained results demonstrate clear benefits of ANN-based THz images processing.

2. Experiment setup for the image data

In total, 15 different samples containing a variety of different objects were processed, which were used for THz imaging. The size of one sample is approximately 15 × 11 cm. There were 6 different object classes: scissors, screwdrivers, pens, knives, guns and lighters put in a random sequence. The samples were made to imitate the non-transparent objects that could be put in an airport bag – one sample containing several objects put in different ways. The objects in the sample were made of aluminum foil, which reflects THz waves well. Additionally, a set of real objects (door keys and screwdrivers) was also imaged, which increases the total number of object classes to 7. The experiment was made by performing transmission measurements in free space via raster scanning, according to the scheme depicted in Fig. 1.

Complementary metal-oxide-semiconductor (CMOS) based field-effect transistor source (*MB Terahercų Technologijos*, Vilnius, Lithuania) emits THz radiation which is collimated and focused onto the sample by high density polyethylene (HDPE) lenses with 6 cm focal distance, L1 and L2, respectively. The light that has passed through the sample is focused onto a broadband THz CMOS detector (*MB Terahercų Technologijos*, Vilnius, Lithuania) using another pair (L3 and L4) of the HDPE lenses. A filter is added to suppress the main, 84 GHz harmonic, and uses only 253 GHz, the third harmonic of the source. Motorized stages were used to move the samples along *x* and *y* axes, with a step size of 1.5 mm. High

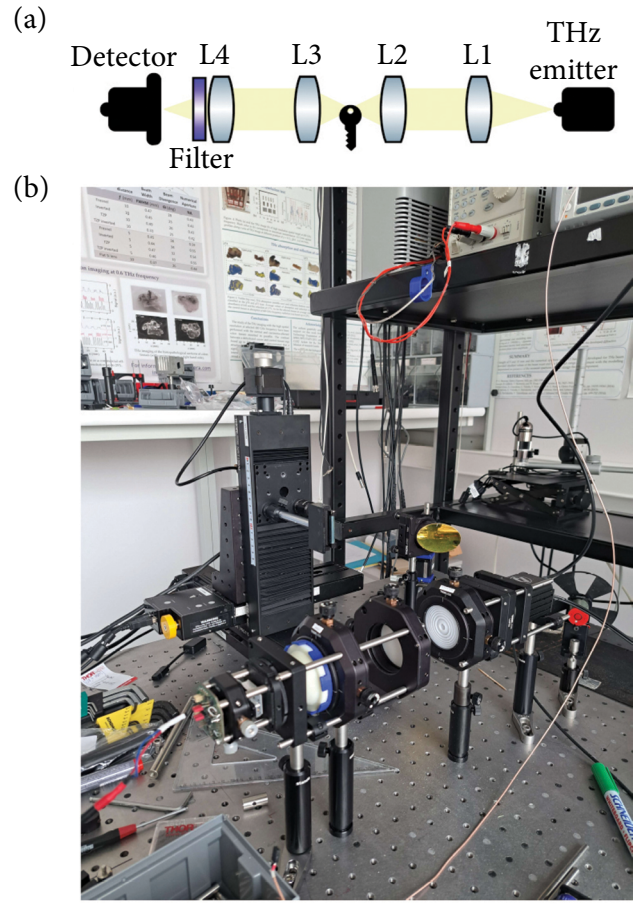

Fig. 1. (a) Raster scan experiment scheme for transmission measurements, where L1, L2, L3 and L4 are HDPE lenses. (b) Picture of the real-life system which was used for the experiment.

resolution images for the uncovered samples were taken with a step size of 1 mm. The obtained image dataset contains 267 raw images, out of which 10 are high resolution images, 166 low resolution and/or concealed images and 91 are images of real objects (keys and screwdrivers). An example of an imaged sample in THz radiation as well as the corresponding photo in visible light are presented in Fig. 2(a, b), respectively.

Materials used to cover the samples are listed in Table 1 along with corresponding refractive indices, absorption coefficients, and thicknesses. They were chosen to represent the popular solutions for packaging. Refractive indexes and absorption coefficients of each material used were found by time-domain terahertz spectroscopy. A femtosecond fiber laser (Femtofiber Pro, *Toptica*, Munich, Germany) provides pulses of 780 nm wavelength and 90 fs pulse duration, and 150 mW output power at 80 MHz pulse repetition rate was used to excite photoconductive antenna made from a 350 μm-thick LT-GaAs wafer. A THz emitter antenna (*Teravil Ltd.*, Vilnius, Lithuania) had the shape of a coplanar line made from Ti/Au with a width of 20 μm and a gap of 50 μm between electrodes. An 8 mm thick and 12 mm in diameter high resistivity hyperhemispherical silicon lens with a focal distance of 500 μm was used to collimate the THz radiation. The THz detector was a Hertzian dipole type photoconductive antenna made from LT-GaAs with a 6 μm wide gap. The emitter exhibits a wide emission spectrum ranging from 0.1 to 5 THz. The scheme of the experiment is presented in Fig. 3.

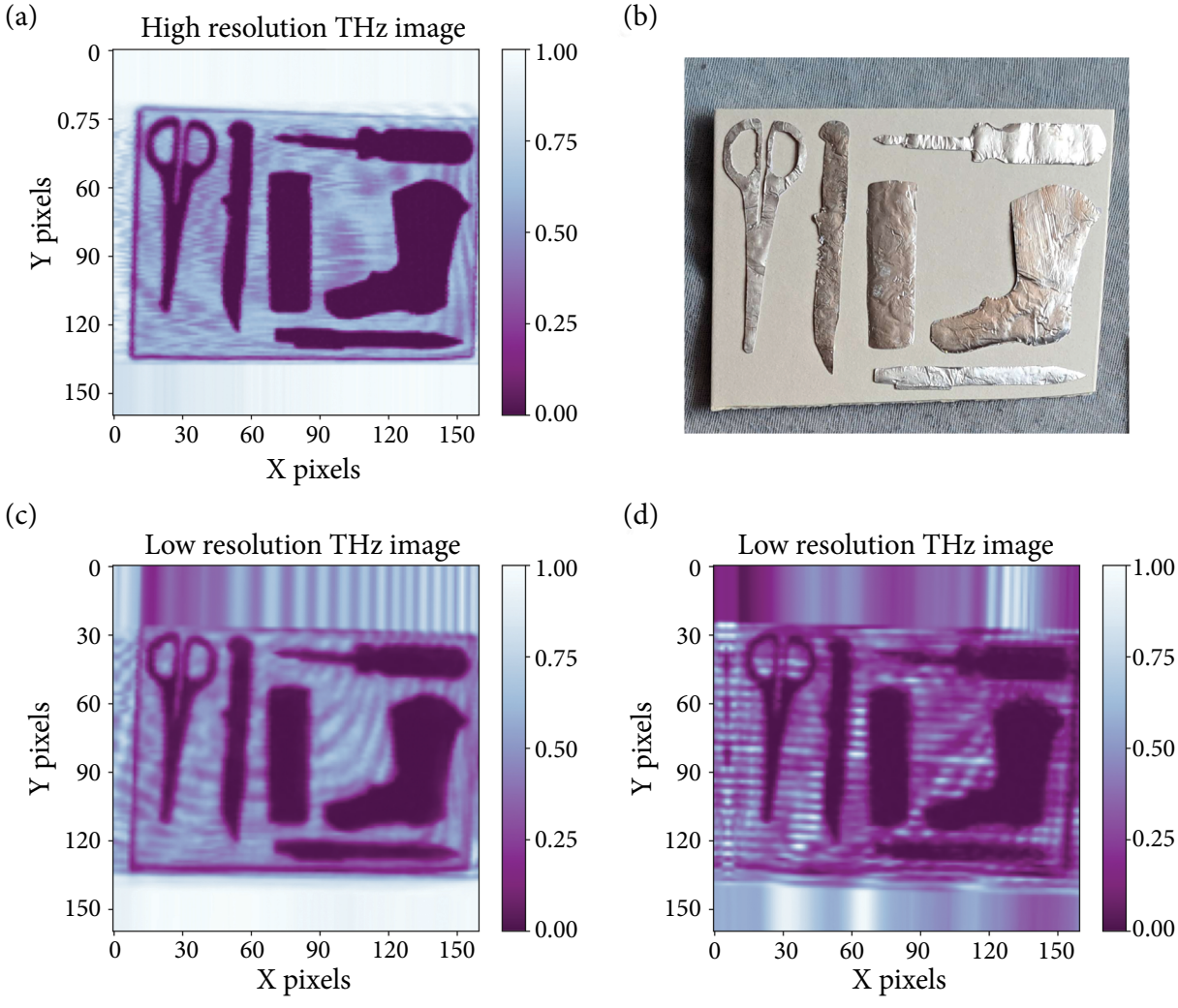

Fig. 2. (a) A high resolution THz image, where the scanning step size is 1 mm; (c) a lower resolution (step size 1.5 mm) THz image. (b) Image of the sample as seen in visible light. (d) THz image of the sample covered with polycarbonate, imaged in a lower resolution case.

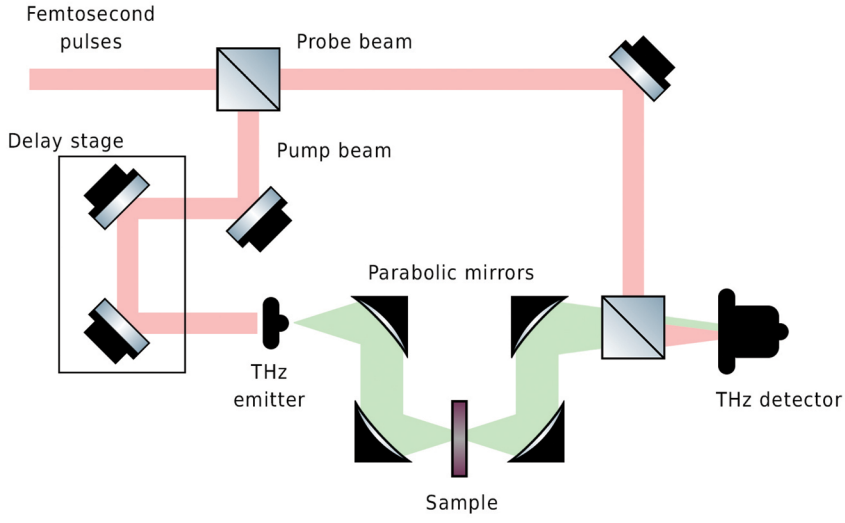

Fig. 3. The arrangement of terahertz time-domain spectroscopy (THz-TDS) system which was used to obtain optical characteristics of the materials listed in Table 1.

Table 1. All the materials that were used to cover the samples for the THz imaging experiment.

Material	Absorption coefficient, cm^{-1}	Refractive index	Thickness, mm
Fabric	0.084	1.025	5.65
Metal mesh	–	–	–
Bubble wrap	0.047	1.021	3.75
Foam rubber	0.828	1.044	10.20
Wood fiber	1.491	1.181	2.91
Polycarbonate	2.412	1.037	4.10
Plywood	3.469	1.362	4.35
EPS foam	0.004	1.009	10.90

3. Material classification

To classify the covering materials, a simple 3-layer convolutional neural network model was used. In total, the model was trained with 9 different classes – all the packaging materials mentioned in Table 1 with the addition of a no-cover class. Images presented to the model were of a single channel (monochromatic), normalized, and resized to 160 × 160 pixels (with additional padding if needed). The complete dataset for this task contained 90 images for training and 48 images for testing. To prevent overfitting such a small dataset, data augmentation methods were used, which included vertical and horizontal flip, random rotation, Gaussian noise, image translation, and zoom. The model reached 83.33% accuracy, with a confusion matrix shown in Fig. 4 for the testing set, which contained images previously unseen by the model.

4. Resolution enhancement

Even though THz waves can penetrate the packaging materials mentioned before, the visual

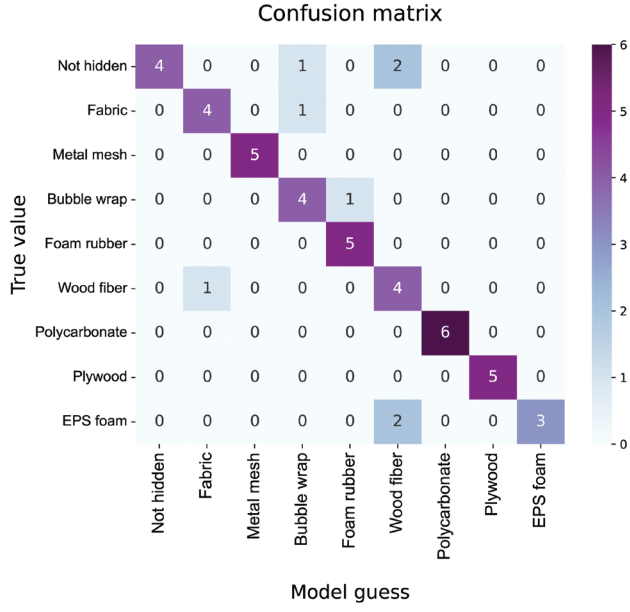

Fig. 4. Confusion matrix for the material classification model.

clarity of objects in covered samples still suffers – the noise level increases and object edges blend with the background thus making it more difficult to distinguish each individual object. To solve this problem, resolution enhancements have to be used. For this task, the DeblurGan [19] neural network architecture was applied. For each low-resolution case, a new generative adversarial network (GAN) [20] model was trained to effectively reduce the different background influence on the objects according to the covering material (9 models in total). The GAN architecture usually consists of two neural network models (generator and discriminator) which compete with each other, producing better results for generating images that represent training data. Each model had 10 high and 10 low resolution single channel image pairs in the training set accordingly. To prevent overfitting, similar data augmentation techniques as before were used, and each model was strictly monitored during training.

Since there is no high-resolution equivalent for the images in the testing set, peak signal-to-noise ratio (PSNR) values were calculated for the training set only (Table 2).

Table 2. PSNR values calculated for each different material. Calculations were made using the training set, since there are no high-resolution cases for testing images.

Material	PSNR, dB
No cover, low resolution	22.44
Fabric	19.07
Metal mesh	17.73
Bubble wrap	21.63
Foam rubber	18.64
Wood fiber	20.02
Polycarbonate	14.67
Plywood	12.45
EPS foam	18.10

Images in the training set, however, were first classified according to the material classification model and then, according to output class, fed to the respective GAN model. Close up example is presented in Fig. 5.

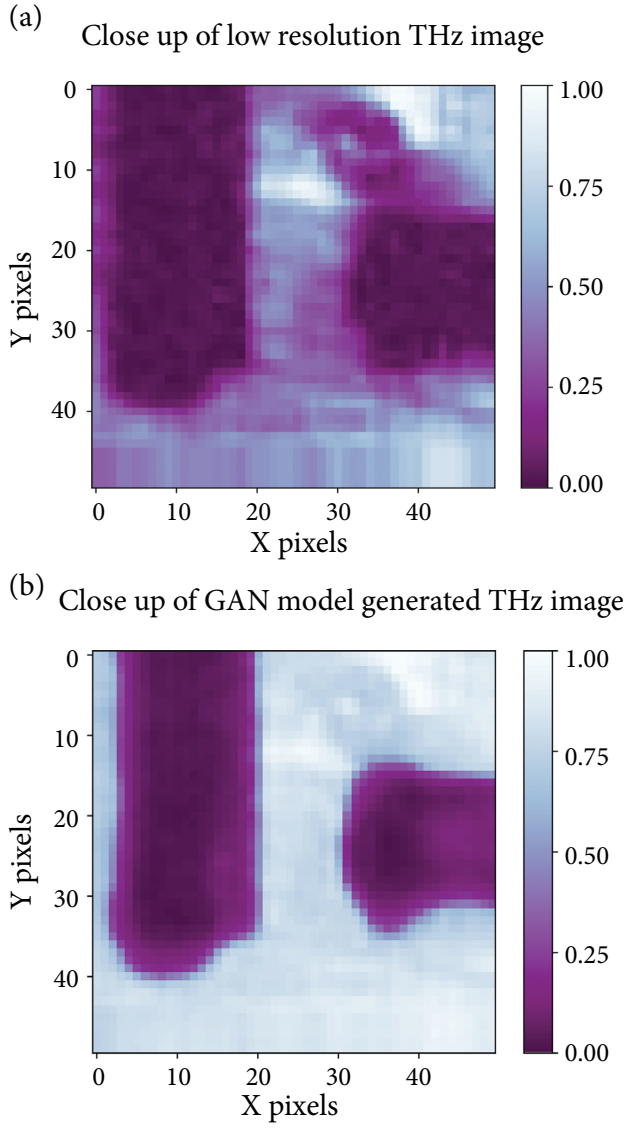

Fig. 5. A close up of (a) low resolution THz image, where objects are hidden by wood and (b) the same THz image edited by a GAN model. The close up presents parts of a lighter and a gun.

5. Object classification

Here, the 3-layer convolutional neural network model was used. In this case, images were split into individual objects, resized and padded if needed to 64 × 64 pixels. Images of real objects and sample splits were joined into one dataset, which has 197 images for training and 775 for testing. The split was chosen in a way that the training dataset would contain high resolution examples, while the testing set has all the low resolution and/or covered cases. The testing data were given to a classification model in two different ways: training set 1 contains images that were edited by the trained GAN models

and set 2 contains raw images of the objects. As mentioned before, there are 7 object classes overall. Since in real life scenarios the visibility of individual objects can become complicated, for example, besides being hidden by various materials, they can also overlap with each other. To account for these cases the data augmentation methods were used. Besides the methods mentioned before, Gaussian blur and random change of contrast were added to simulate effects that covering objects with different materials have. Furthermore, random size blobs in random locations were generated to account for the cases where the object of interest is covered by another secondary object. The accuracy of the model was tested in two cases – case 1 contains images which have their resolution changed by one of the respective GAN models, while case 2 contains images which were not edited in any way. Case 1 reached 89.42% overall prediction accuracy, while case 2 reached 81.03% prediction accuracy. Confusion matrices for both cases are presented in Fig. 6. Precise accuracy values for each material are presented in Table 3.

Table 3. Summary of accuracies based on a specific material that covers classifiable objects.

Material	Accuracy, test set 1	Accuracy, test set 2
Fabric	86.7%	88.9%
Metal mesh	90.0%	91.1%
Bubble wrap	91.1%	87.8%
Foam rubber	88.9%	92.2%
Floor-cover	95.0%	90.0%
Polycarbonate	89.5%	76.8%
Plywood	88.9%	31.1%
EPS foam	93.3%	89.9%

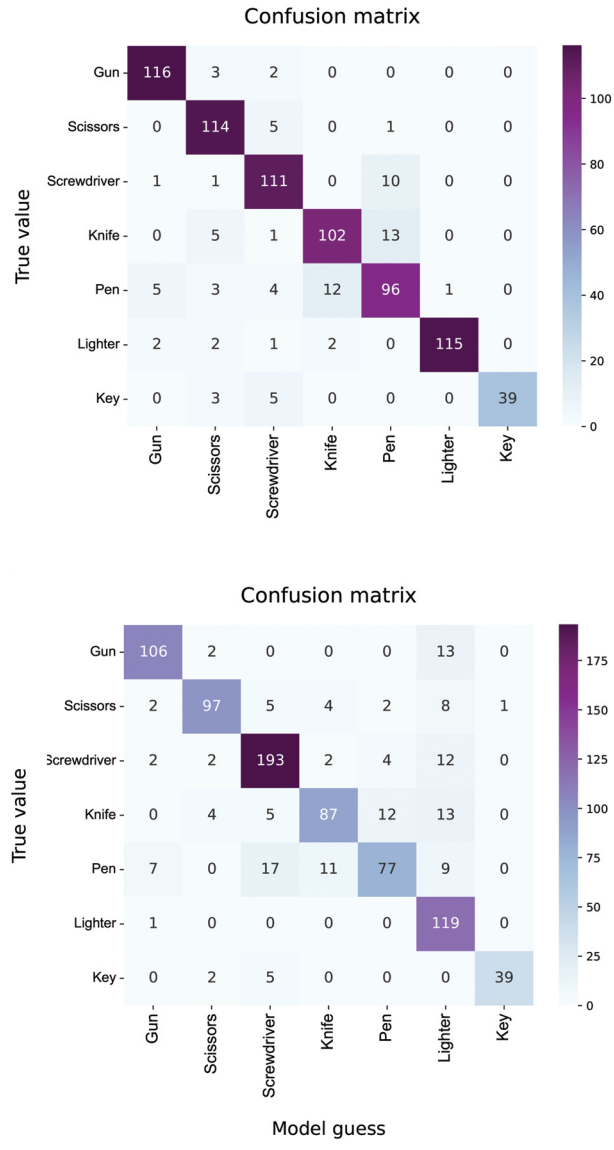

Fig. 6. (a) Confusion matrix for the classification model using the first testing set, where images were edited with a respective material GAN network. (b) Confusion matrix for the classification model using a second testing set that contains raw, unedited images.

6. Discussion

The 83.33% prediction accuracy for classifying materials shows that material recognition could be still improved. The confusion matrix depicted in Fig. 4 shows that the best classified materials provide strong visual traits – metal mesh has a clear grid pattern, polycarbonate has stripes, and wood absorbs the most amount of radiation. The materials that are misclassified do not have distinct similarities in their absorbance coefficients or refractive indices. Even though there are cases where misclassified materials have similar refractive indexes (fabric, which was classified as bubble wrap), most of the mismatched cases have no direct correlation between the model output class and their optical properties. This means that while classifying, neural network models rather consider visual properties of those materials than optical ones.

After classifying the materials, images are then put into a respective GAN model, which should improve the quality. Generally, even if the material

is wrongly identified, the result is still positive, as a respective GAN model still manages to decrease the background influence and thus the object itself is better visible than in the original picture. Though the quality of GAN output depends on a material, if the original low-resolution image is similar to high resolution image, the model will produce good results with higher probability. This can be seen from Table 2, as the model that reached the highest PSNR value takes non-covered objects as an input, while the model with the lowest PSNR value takes objects covered by wood as an input; this material has higher absorption than the rest and therefore the highest background influence. In this case, PSNR values also do not have any correlation with the physical properties of materials.

During the object classification, objects that had their resolution previously improved by a respective GAN model reached higher (89.42%) accuracy than unedited ones (81.03%). From confusion matrices (Fig. 6) it can be seen that the most often misclassified objects (pens, screwdrivers and knives) have a similar distinctive shape (Fig. 7): they are all long and thin, thus, with no colour or other supplementary information it is difficult to distinguish between them.

Another observation is that in the second test set, lighter class is guessed significantly larger number of times than in the first test set, which might be due to bigger background influence on the image – it is too difficult to separate the object form the background, and the shade that looks like a noisy rectangular box might be perceived by the model as lighter class.

Furthermore, the question arises whether it is beneficial to edit images with GAN models in all material cases. Referring to Table 3, one can see that in most cases, after editing the picture with a respective GAN, the accuracy increases significantly, for instance, in the wood case, the difference in accuracy is above 50%. On the other hand, there are cases which have lower accuracy (up to 4%) after editing them with GAN models, namely fabric, metal mesh, and foam rubber. Though the difference is not large (less than 4%), it is worth mentioning.

7. Conclusions

In this work, three different databases of THz images for training and testing neural network models were created and used in concealed object classification. The first problem that was tackled is material classification – the accuracy of 83.33% was reached, while classifying material from single channel THz images only and using a convolutional neural network model without any additional information. Furthermore, as THz images, especially those that capture objects covered in different packing materials, have a low resolution and are blurry, nine different GAN models were trained, which were meant to improve the low-resolution THz images based on each material class. The GAN models successfully decreased the background influence in the images that led to improved object classification, which reached 89.42% of overall accuracy, while the classification of raw low-resolution THz images was performed with 81.03% accuracy.

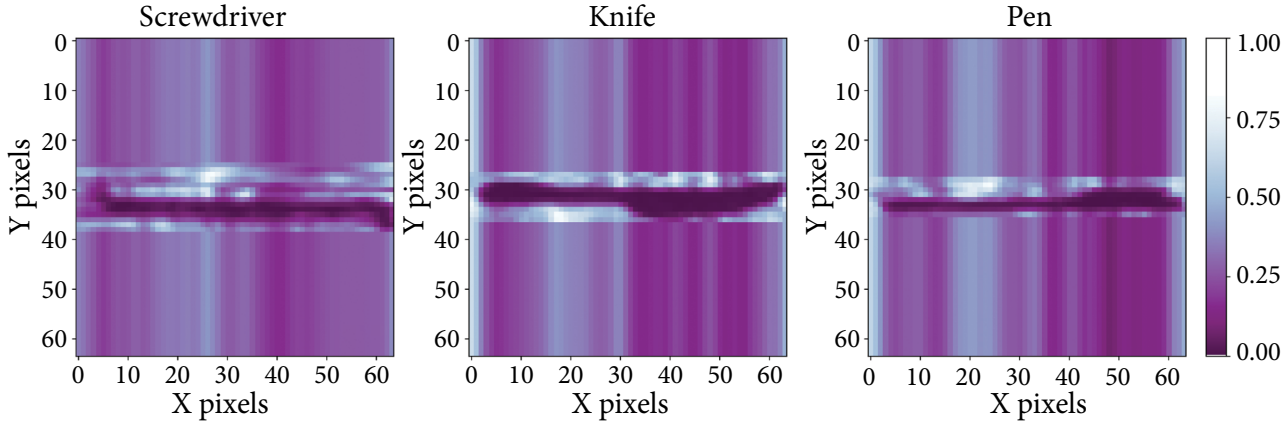

Fig. 7. Examples of registered THz images: screwdriver, knife and pen. All of those images were classified wrongly.

The PSNR metric of images with improved resolution reached up to 22.44 dB. Also, refraction indices and absorption coefficients of the covering materials were found using the THz-TDS technique. It was found that the accuracy of object and material classification generally does not depend on the optical properties of covering material.

Acknowledgements

We would like to express our gratitude to dr. Andrzej Urbanowicz for the measurements with the THz time-domain setup.

References

[1] A. Leitenstorfer, A.S. Moskalenko, T. Kampfrath, J. Kono, E. Castro-Camus, K. Peng, N. Qureshi, D. Turchinovich, K. Tanaka, and A. Markelz, The 2023 terahertz science and technology roadmap, J. Phys. D **56**, 223001 (2023).

[2] X. Li, J. Li, Y. Li, A. Ozcan, and M. Jarrahi, High-throughput terahertz imaging: progress and challenges, Light Sci. Appl. **12**, 233 (2023).

[3] R. Piesiewicz, C. Jansen, S. Wietzke, D. Mittleman, M. Koch, and T. Kürner, Properties of building and plastic materials in the THz range, Int. J. Infrared Milli. Waves **28**, 363–371 (2007).

[4] A. Nakanishi and H. Satozono, Terahertz optical properties of wood–plastic composites, Appl. Opt. **59**, 904–909 (2020).

[5] A. Prokscha, F. Sheikh, K. Kolpatzeck, Y. Zantah, D. Lessy, J. Balzer, A. Czylwik, and T. Kaiser, Terahertz insights into fabric look-through, in: *Proceedings of 2024 15th German Microwave Conference* (IEEE, 2024) pp. 241–244.

[6] T.S. Hartwick, D.T. Hodges, D.H. Barker, and F.B. Foote, Far infrared imagery, Appl. Opt. **15**, 1919–1922 (1976).

[7] B.B. Hu and M.C. Nuss, Imaging with terahertz waves, Opt. Lett. **20**, 1716–1719 (1995).

[8] A.G. Davies, A.D. Burnett, W. Fan, E.H. Linfield, and J.E. Cunningham, Terahertz spectroscopy of explosives and drugs, Materials Today **11**, 18–26 (2008)

[9] T. Mohr, S. Breuer, G. Giuliani, and W. Elsäßer, Two-dimensional tomographic terahertz imaging by homodyne self-mixing, Opt. Express **23**, 27221–27229 (2015).

[10] K. Komatsu, T. Iwamoto, H. Ito, and H. Saitoh, THz gas sensing using terahertz time-domain spectroscopy with ceramic architecture, ACS Omega **7**, 30768–30772 (2022).

[11] Y. Peng, C. Shi, X. Wu, Y. Zhu, and S. Zhuang, Terahertz imaging and spectroscopy in cancer diagnostics: A technical review, BME Front. **25**, 2547609 (2022).

[12] K. Ikamas, D.B. But, A. Cesiul, C. Kołaciński, T. Lisauskas, W. Knap, and A. Lisauskas, All-electronic emitter-detector pairs for 250 GHz in silicon, Sensors **21**, 5795 (2021).

[13] A. Siemion, L. Minkevičius, L. Qi and G. Valušis, Spatial filtering based terahertz imaging of low absorbing objects, Opt. Lasers Eng. **139**, 106476 (2021).

[14] Y. Freund and R.E. Schapire, Large margin classification using the perceptron algorithm, Mach. Learn. **37**, 277–296 (1999).

[15] A. Derry, M. Krzywinski, and N. Altman, Convolutional neural networks, Nat. Methods **20**(9), 1269–1270 (2023).

[16] D. Liang, F. Xue, and L. Li, Active terahertz imaging dataset for concealed object detection (2021), arXiv:2105.03677v1

[17] Y. Li, W. Hu, X. Zhang, Z. Xu, J. Ni, and L.P. Ligthart, Adaptive terahertz image super-resolution with adjustable convolutional neural network, Opt. Express, **28**, 22200 (2020).

[18] Z. Long, T. Wang, C. You, Z. Yang, K. Wang, and J. Liu, Terahertz image super-resolution based on a deep convolutional neural network, Appl. Opt., **58**, 2731 (2019).

[19] O. Kupyn, V. Budzan, M. Mykhailych, D. Mishkin, and J. Matas, DeblurGAN: Blind motion deblurring using conditional adversarial networks, in: *Proceedings of 2018 IEEE/CVF Conference on Computer Vision and Pattern Recognition*, 8183 (IEEE, 2018), arXiv:1711.07064v1.

[20] A. Thakur, Generative adversarial networks, Int. J. Res. Appl. Sci. Eng. Technol. **9**, 2307–2325 (2021).

PASLĖPTŲ OBJEKTŲ KLASIFIKACIJA NAUDOJANT TERAHERCINĮ VAIZDINIMĄ IR DIRBTINIUS NEURONINIUS TINKLUS

U. Šilingaitė, I. Grigelionis

Fizinių ir technologijos mokslų centras, Vilnius, Lietuva

Santrauka

Terahercinį (THz, bangos ilgiai 0,3–3 mm) vaizdinimą galima taikyti daugelyje sričių, pavyzdžiui, medicinoje, kokybės kontrolės ar saugumo srityse, nes šio dažnio bangos gali prasiskverbti pro įvairias dielektrines medžiagas. Tačiau THz vaizdams būdinga maža vaizdo raiška ir didelis triukšmas, todėl sudėtinga panaudoti šį bangos ilgį objektų atpažinimui ir klasifikavimui. Šią problemą galima spręsti pasitelkiant dirbtinius neuroninius tinklus, gebančius apdoroti vizualinę informaciją. Šiame darbe objektų vaizdų duomenų bazė buvo surinkta naudojant monochromatinę 253 GHz dažnio spinduliuotę. Vaizdinami objektai buvo arba atviri, arba uždengti įvairiomis pakavimo medžiagomis. Surinkta duomenų bazė buvo naudojama skirtingiems neuroniniams tinklams apmokyti, kurie atlieka tris užduotis: (i) klasifikuoja objektus; (ii) gerina vaizdo kokybę; (iii) klasifikuoja objektus dengiančias pakavimo medžiagas. Gauti rezultatai parodė, kad pakavimo medžiagos yra klasifikuojamos 83,33 % tikslumu, o individualūs objektai – 89,42 % tikslumu. Vaizdų raiškos gerinimas priklauso nuo pakavimo medžiagos, o geriausia gauta signalo ir triukšmo santykio vertė siekia 22,44 dB. Naudojant THz-TDS sistemą nustatytos pakavimo medžiagų optinės savybės, tačiau tyrimo metu paaiškėjo, kad jos nekoreliuoja su objektų ir medžiagų klasifikacijos rezultatais.